GEOPHYSICS, VOL. 73, NO. 5 (SEPTEMBER-OCTOBER 2008); P. VE173–VE181, 17 FIGS.
10.1190/1.2966096

Advances in velocity model-building technology for subsalt imaging

Bin Wang[1], Young Kim[1], Chuck Mason[1], and Xiansong Zeng[1]

ABSTRACT

Seismic imaging of hydrocarbon accumulations below salt is a formidable challenge because complexly shaped salt bodies severely distort wavefronts or scatter seismic energy. We have highlighted some recent advances in building a velocity model for subsalt imaging. There are three main stages: suprasalt velocity determination, salt-model definition, and subsalt velocity update. Volumetric high-resolution tomography that incorporates high-velocity contrast boundaries is used to derive a good sediment velocity model before building a salt model. To facilitate integration of interpretation and depth processing, beam-based interactive imaging is used to refine the salt geometry. For subsalt velocity update, either subsalt tomography or subsalt scan-based techniques can be used, depending on the quality of subsalt reflections. There are concepts and techniques for attaining subsalt images suitable for hydrocarbon exploration beneath complexly shaped salt bodies.

INTRODUCTION

Prestack depth migration has been used routinely for subsalt imaging in the Gulf of Mexico. To produce a good subsalt image, an accurate velocity model is needed. Generation and refinement of a velocity model in a routine production project are often a complex process (Singer, 2005). The model typically has multiple embedded salt bodies of complex geometries. Building the velocity model often occurs in three stages: suprasalt velocity estimation using grid tomography, salt-geometry definition, and subsalt velocity model building. Each stage often includes many internal iterations.

An accurate suprasalt sediment velocity model is critical to the subsequent definition of salt geometry. The standard method to derive such a model is tomography based on residual moveouts in prestack depth-migration (PSDM) gathers (Stork, 1992; Wang et al., 1995; Zhou et al., 2001; Guillaume et al., 2003). Field data examples in the literature (e.g., Dirks et al., 2005) show that high-resolution, grid-based tomography using automatic, dense, and volumetric residual-moveout picking is an effective method, especially for areas in the Gulf of Mexico where sediment velocities are driven primarily by compaction. More recently, hybrid grid tomography (Campbell et al., 2006) was proposed to incorporate boundaries with high velocity contrasts (e.g., carbonate layers). This methodology allows us to better define velocity models for data with increasingly complex geology.

In the recent special issue of THE LEADING EDGE focusing on subsalt exploration (November 2007), the need for accurate interpretation of salt and salt-model building was emphasized (Sayers and Herron, 2007; Mosher et al., 2007). Identification and definition of salt geometry are critical and time-consuming steps necessary for successful subsalt imaging. Reasnor (2007) pointed out that salt interpretation can account for about 70% of a typical depth-imaging project.

The process of salt-model building and prestack depth migration is iterative, and it requires integration of salt interpretation and depth processing. Salt interpretation is not straightforward for a complex salt geometry. It requires testing different scenarios, especially for the base of salt (BOS), where the quality of images often is poor. Because of the iterative nature of depth imaging and velocity model building, it often is desirable to develop fast depth-migration algorithms for velocity model building (Wang and Pann, 1996; Sun et al., 2000; Hua and McMechan, 2001, 2003; Sun and Schuster, 2003; Fei and McMechan, 2006).

Beam-based migration (Hill, 1990; Gray, 2005) can be used for complex salt-model building because of its steep-dip imaging and multipathing capabilities and its speed, which is much faster than wave-equation migration. Gao et al. (2006) attempted to integrate salt interpretation and velocity model building with fast beam migration. They demonstrated that fast beam migration could serve as an interactive imaging tool for subsalt velocity model building. Because subsalt velocity model building depends heavily on an accurate definition of salt geometry, it is imperative for interpreters to have tools for testing different salt geometries. We show the use of fast beam migration as an interactive imaging tool for refining BOS interpretation.

Manuscript received by the Editor 27 December 2007; revised manuscript received 18 March 2008; published online 1 October 2008.
[1]TGS, Houston, Texas, U.S.A. E-mail: bwang@tgsnopec.com; ykim@tgsnopec.com; cmason@tgsnopec.com; xzeng@tgsnopec.com.

After defining the salt geometry, we face the challenging task of updating subsalt velocities. Subsalt reflections often are very weak and severely intermingled as a result of complexly shaped salt bodies. Recently, wavefield redatuming approaches (Schuster and Zhou, 2006; Wang et al., 2006a; Liu et al., 2007; Lu et al., 2007) have been proposed to ease the task of subsalt velocity model building. It is advantageous to redatum the wavefield below complex salt bodies (or through the salt bodies, if the BOS is not finalized yet). Because the wavefield will be simplified greatly (Wang et al., 2006) by redatuming, more efficient migration algorithms can be used for subsalt velocity analysis. In addition, the wavefield is closer to subsalt targets so that a smaller migration aperture is sufficient, which reduces the cost of migration.

Subsalt velocity update (Wang et al., 2004; Wang et al., 2006a) can be categorized into two approaches: (1) data-driven subsalt tomography based on residual moveouts, and (2) interpretation-driven subsalt wave-equation migration (WEM) scans (Wang et al., 2006b). When subsalt reflections are defined well and their reflection angle range is broad, subsalt tomography works just as well as suprasalt tomography. However, if subsalt reflections are not defined well or if the range of reflection angle is limited, we might have to rely on a brute-force approach such as subsalt WEM scan.

Although subsalt WEM scan is effective, the cost of generating migration scans is still comparatively high. To address the cost issue, two efficient alternatives for subsalt scan have been proposed: demigration followed by poststack migration scan (Wang et al., 2005b) and focusing analysis based on a delayed-imaging-time (DIT) scan (Wang et al., 2005a; Wang et al., 2006). In this paper, we will show field data examples of these alternative subsalt scanning techniques.

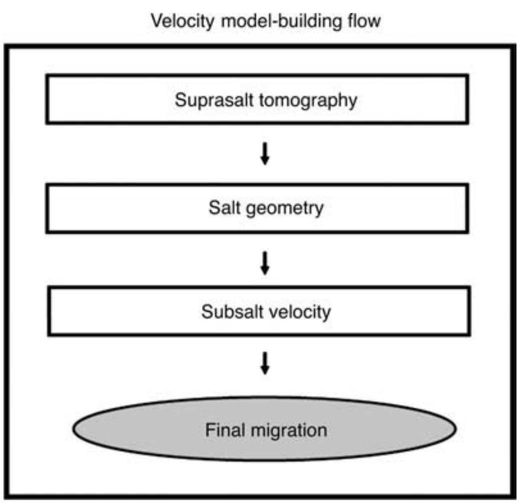

Figure 1. Simplified processing flow for a typical subsalt imaging project. The first three steps of the flow might be iterated a few times before final migration.

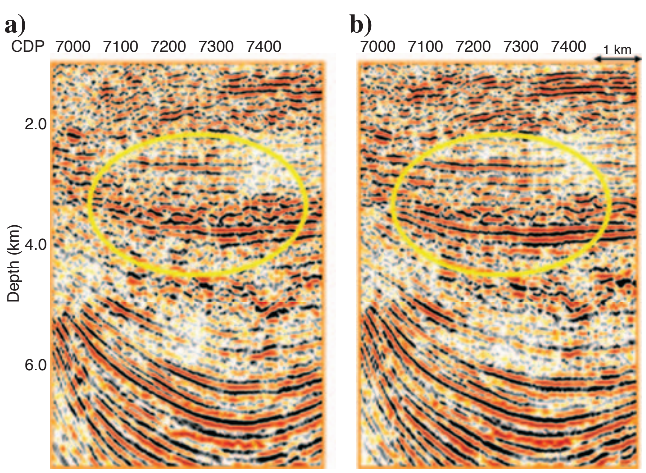

Figure 2. Comparison of prestack depth migration images (a) before and (b) after sediment tomography. After tomography, the focusing and continuity of events are improved at the middle of the section.

SUPRASALT TOMOGRAPHY

Figure 1 shows a simplified flow for subsalt imaging. For suprasalt velocity modeling, we use 3D grid tomography (e.g., Epili et al., 2007) to estimate velocities above the salt. Figure 2 shows the prestack depth-migration images before and after our 3D grid-based tomography. Figure 3 shows the common-image-point (CIP) gathers before and after 3D sediment tomography. After tomography, it is clear that events are more continuous on the stack sections and gathers are flattened better across the offset range. These results indicate a more accurate image, assuming an isotropic velocity field.

Although grid tomography is an efficient way to determine velocities in areas where velocity gradients are mild, it is not very effective when dealing with sharp velocity contrasts. A hybrid velocity-model representation that incorporates layer constraints in the model is more effective when dealing with layers such as chalk or carbonate, which have high velocity contrasts (Campbell, 2006). Figures 4 and 5 show an example of hybrid tomography applied to data from the Santos Basin offshore Brazil.

The velocity model shown in Figure 4a was derived by regular grid tomography. Because of regularization in grid tomography, it failed to preserve the sharp velocity discontinuity caused by a carbonate layer (indicated by a red curve in Figure 5a). Figure 5a shows

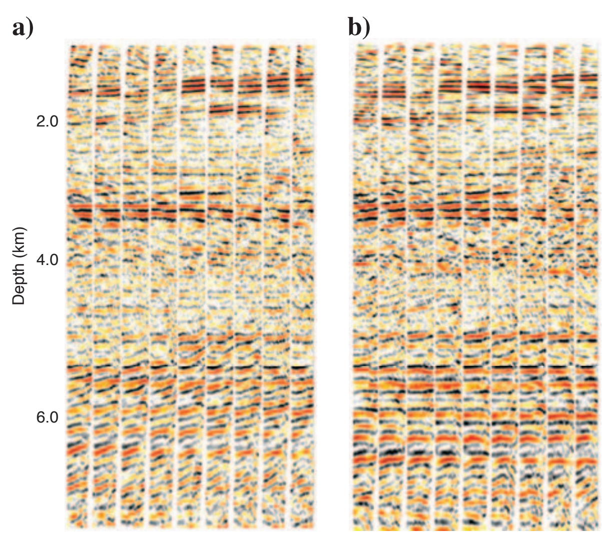

Figure 3. Common-image-point gathers (a) before and (b) after sediment tomography. Events in the gathers are flatter after tomography, indicating a more accurate velocity model, assuming an isotropic velocity field.

a PSDM image using the model displayed in Figure 4a. Although the reflectors are focused fairly well, the base of salt (the brightest reflector in the middle of the image) is distorted badly and mimics the top of carbonate. We introduced a layer constraint into the model to preserve the top of the carbonate layer, and we allowed grid tomography to detect lateral velocity changes within the carbonate layer.

A velocity model using hybrid tomography is shown in Figure 4b, which preserved the sharp velocity change across the top of the carbonate layer and solved lateral variations within the layer. A salt layer underneath the carbonate layer is not discernible because of the small velocity contrast between them. Figure 5b shows the PSDM image using the velocity model derived by hybrid tomography. Because of the preserved velocity contrast at the top of the carbonate layer, the base of the salt does not mimic the top of the carbonate layer, which is consistent with the regional geology. In addition, the reflectors within the carbonate layer are enhanced further because lateral velocity variations within the layer are resolved better.

SALT-MODEL BUILDING

Once the velocities above the salt are determined, it is relatively straightforward to pick the top of the salt. However, it often is difficult to define the base of salt because of lack of reflections or interference with noise, such as residual multiples. Although the base of salt might not be visible in an image, there are many cases in which subsalt reflections are discernible (for example, see Figure 6a). In such cases, one can test many scenarios for the base of salt and define the salt geometry based on the continuity or geologic consistency of subsalt reflectors. Because the data must be migrated many times using different salt geometries, it is desirable to have a fast migration tool which allows the testing of many scenarios. In this section, we describe an approach that combines demigration and fast beam migration.

Fast beam migration has been reported as a tool for fast migration (Gao et al., 2006; Fei and McMechan, 2006). In addition, Fei et al. (2006) demonstrate that residual moveouts (RMOs) of fast beam migration can match those of Kirchhoff migration so that RMOs of fast beam migration can be used for tomography. However, the quality of fast beam migration depends greatly on the validity of dips determined by dip scan. It is particularly difficult to determine dips in the crossline direction in prestack data because of sparse and irregular sampling and poor signal-to-noise ratio (S/N) of subsalt reflections. To enhance the quality of the dips that can be used for fast beam migration, we combined demigration and poststack fast beam migration, which allowed us to test many salt geometries. The use of demigration followed by migrations for velocity modeling has been reported by many authors (for example, Kim et al., 1996; Wang et al., 2005c; Mosher et al., 2007).

Our procedure is as follows: First a PSDM image is demigrated with the same velocity model used for PSDM, placing the reflections at their unmigrated locations. Demigration to a subsurface datum (for example, below a rugose top of salt) is advantageous because subsalt reflections will be closer to their correct migrated locations. Therefore, the amount of conflicting dips will be far less than those in a demigrated wavefield to the surface. In addition, estimating the dips of reflections in the demigrated data enables us to determine dips reliably because the wavefield is specified in a regular and fine grid. Figure 6 shows a PSDM image, the velocity model used for PSDM, and the demigrated wavefield to a datum surface at a depth of 3200 m.

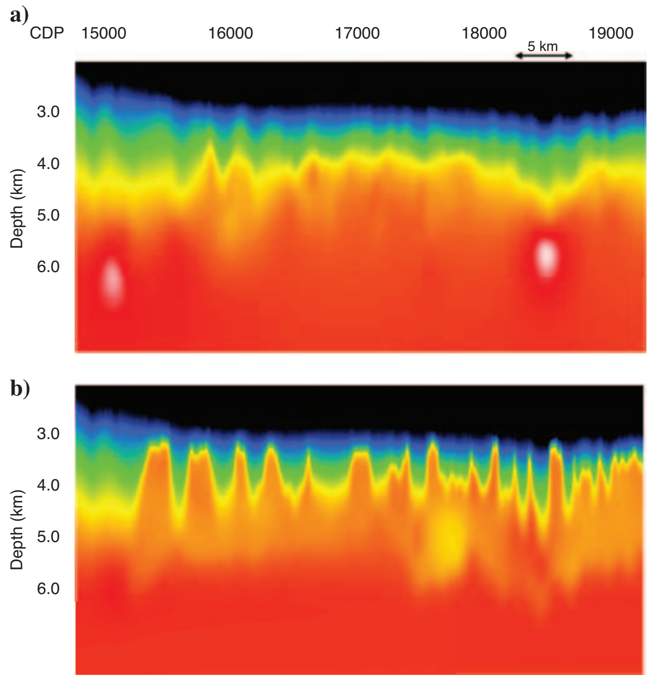

Figure 4. Comparison of sediment velocity models derived by (a) regular grid tomography and (b) hybrid tomography. Hybrid tomography captures sharp velocity contrast boundaries better for the velocity model. In addition, it allows horizontal velocity variation inside the carbonate layer. The vertical exaggeration used is about 10.

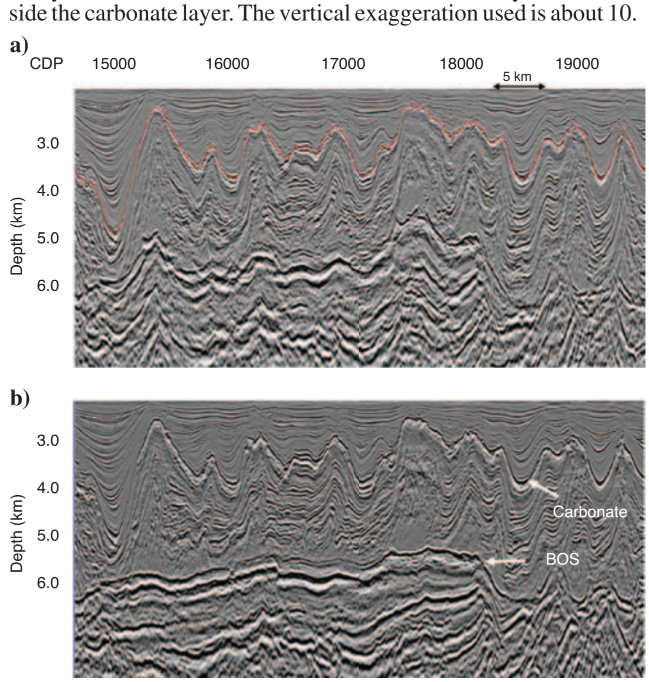

Figure 5. Prestack depth-migration images using (a) regular grid tomography and (b) hybrid tomography. The undulation of the bottom of salt (BOS) in (a) mimics the top of carbonate horizontal depth variation. After hybrid tomography, the subsalt image is focused better, and the BOS shows a more realistic geologic representation.

Next, the dips of reflections in the demigrated data are picked and used for fast beam migration to test salt geometries. Figure 7 shows three salt geometries: the initial salt model, one of the intermediate salt models, and the final salt model. Figure 8 shows beam-migrated images corresponding to the models shown in Figure 7. Note that subsalt reflections in the red circle in Figure 8a display a major discontinuity because of a wrong salt geometry. More salt was added, as shown in Figure 7b, but the discontinuity was not completely mitigated, as shown in Figure 8b.

After testing many geometries, we arrived finally at the model shown in Figure 7c, with the corresponding image shown in Figure 8c. Note that although the reflectors still are broken, possibly because of poor illumination caused by the steep salt flank, their depths are continuous, in agreement with the local geology. The importance of making this process interactive must be emphasized. The main goal of this step is to define salt-body geometry. All subsequent subsalt work is dependent on it.

In areas where interpretation is difficult, a given salt model is tested, and subsequent modifications of that model are based on visualization of its effect. It is critical to maintain continuity of the thought process while testing geometry scenarios. This can be done only with interactive updating of the image. By combining demigration of a PSDM image with a subsurface datum and fast beam migration, we tested many scenarios in an interactive manner, shortening the time needed to define the salt geometry.

After the salt geometry was finalized, we ran a 3D wave-equation-based prestack depth migration using the final velocity model. Figure 9 shows a comparison of the PSDM images using the initial and final models. With the improved salt model, reflectors below the salt are enhanced further, and their continuity is improved. The reflectors still are broken directly below the steep salt flank, possibly because of lack of illumination.

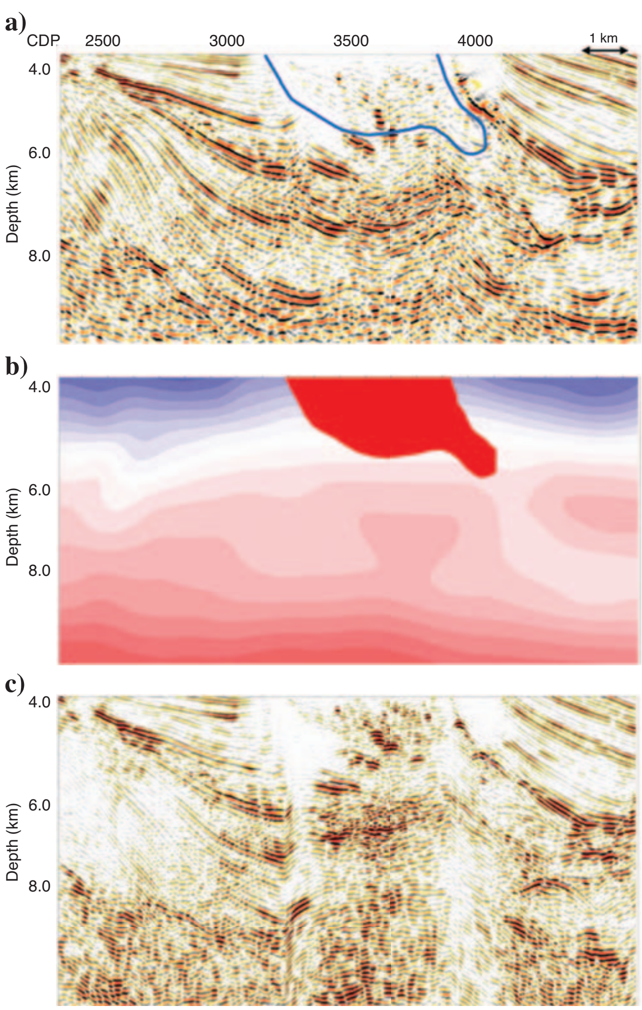

Figure 6. Example showing salt-model geometry refining. (a) The prestack WEM image and (b) the velocity model were used to produce (c) the poststack wave-equation-based demigration result, which was used as input to beam migration. The bottom of salt (BOS) indicated by the curved line in (a) was not well imaged or defined. Demigration regularizes the data and facilitates the picking of BOS.

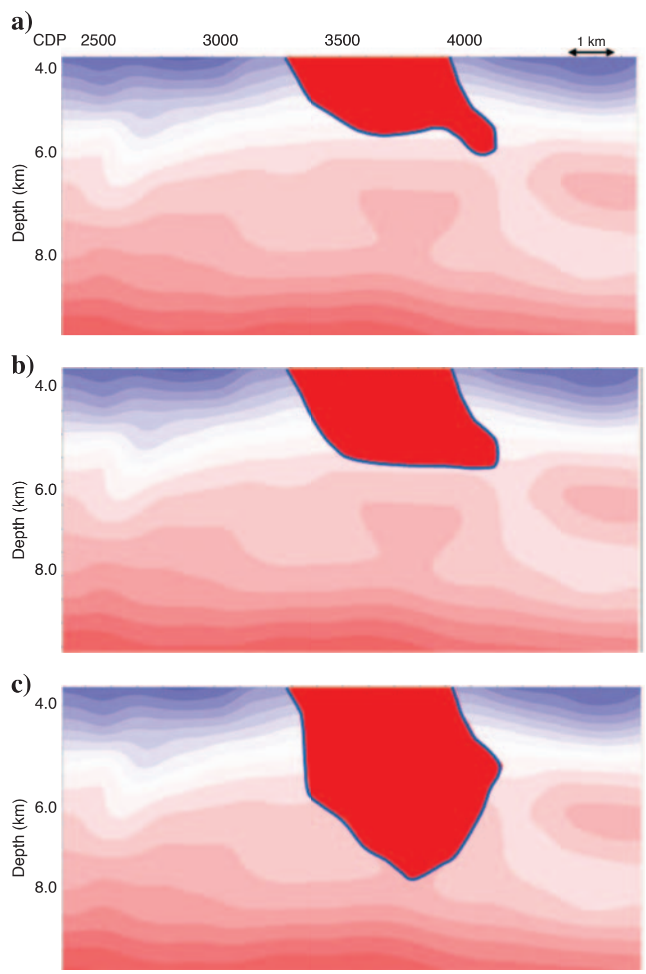

Figure 7. When the bottom of salt (BOS) is not defined well in the migrated image (Figure 6a), different interpretations of the BOS are tested using fast beam migration interactively. Three velocity models used are shown here.

SUBSALT VELOCITY UPDATE

After finalizing the geometry of salt bodies, we still face a challenge in updating velocities below the salt. In this section, we describe two approaches for subsalt velocity update: data-driven subsalt tomography and interpretation-driven migration scan (Wang et al., 2006b). When there are well-focused reflections with a high S/N and a wide range of reflection angle, subsalt tomography often is effective. However, a scan-based method is more effective when the S/N of subsalt reflections is low, making it hard to determine RMOs, or when the range of reflection angle is limited.

Subsalt tomography

Subsalt tomography is fundamentally the same as regular tomography except that as with hybrid tomography, a constraint is introduced so that velocities are not updated above the base of salt. Figure 10 shows an example of subsalt tomography. The top section displays a PSDM image before subsalt tomography, and the bottom section is a PSDM image after tomography. The images are overlaid with corresponding velocity models. Note that reflectors below the salt were focused far better, and their continuity was improved. Velocities just below salt were reduced by 10% by subsalt tomography, and velocities farther below salt were increased as a result of carbonate layers in the surrounding area.

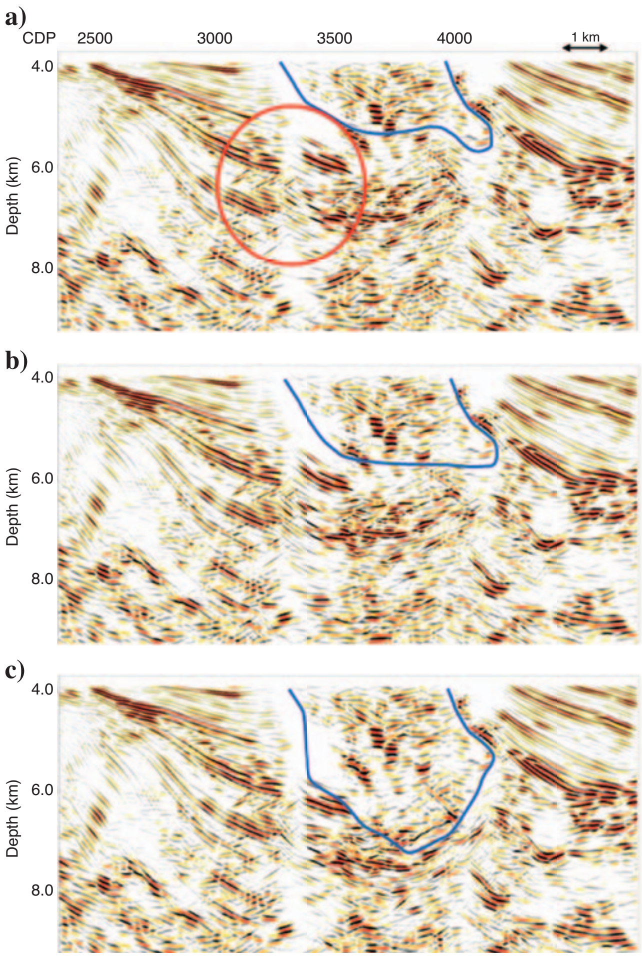

Figure 8. Three migration images correspond to the three velocity models shown in Figure 7 obtained by fast beam migration. The interactive nature of fast beam migration allows the bottom of salt to be defined progressively and quickly.

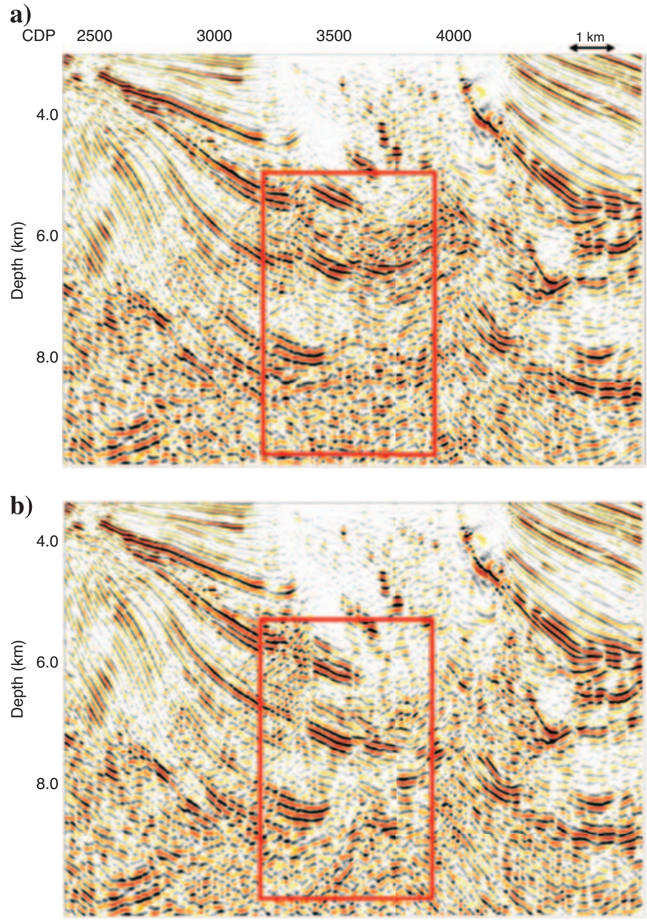

Figure 9. Prestack WEM images using (a) initial velocity model in Figure 7a and (b) final velocity model in Figure 7c. The subsalt image is improved greatly in (b).

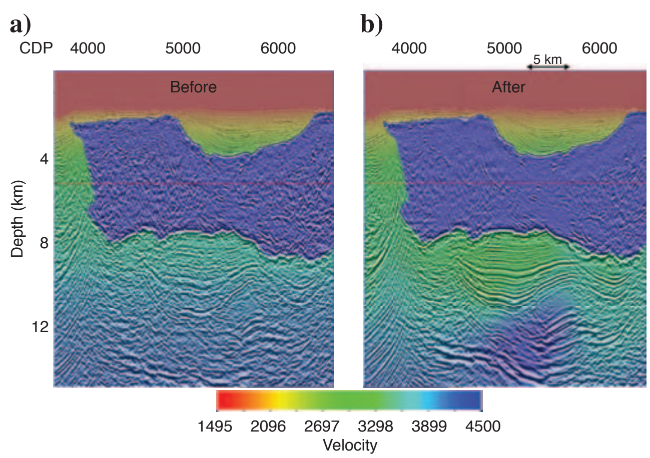

Figure 10. Prestack WEM images with velocity overlay (a) before and (b) after subsalt tomography. In the poor S/N subsalt area on the left, tomography was unable to improve the image significantly.

Figure 11 shows the comparison of CIP gathers before and after subsalt tomography. Before tomography, events in the image gathers are undercorrected, indicating that velocities were too high. After tomography, events in CIP gathers are flatter and appear shallower because of the decrease in subsalt velocity.

WEM-scan-based subsalt velocity update

When subsalt reflections are imaged poorly or the range of reflection angle is limited, tomography-based methods are not effective for updating subsalt velocities. In such cases, we might have to rely on a more direct approach such as WEM scan. Before employing WEM-scan-based velocity update, one must define correctly the salt geometry, which has a stronger impact than subsalt sediment velocities because of severe velocity contrasts. Otherwise, subsalt velocity update might try to compensate for errors in the salt model.

Both subsalt tomography and WEM scan are applied independently for this area. In this example, WEM-based subsurface angle gathers are used for subsalt tomography. Because of a limited reflection angle range and the low-frequency content of wave-equation migration images, the picked subsalt RMOs were not reliable. After two iterations of subsalt tomography, we obtained only marginal improvement of the subsalt image. This necessitated a more expensive WEM-scan-based update, with its advantages of stack power and ability to view the migrated images. Because of the questionable validity of the RMO picks and subsequent results of subsalt tomography, the tomography update was not used for the WEM-scan flow. Errors introduced by tomography can hinder the ability to converge on the correct velocity model.

To reduce the cost of generating prestack subsalt WEM scans, we used common-P (or delayed-shot) wave-equation migration instead of common-shot migration. Because the goal of subsalt scan is to capture image quality differences for different velocity models, we could reduce the computational cost by using a smaller number of Ps for migration, particularly when subsalt reflectors have gentle dips. The number of Ps can be reduced by limiting the range of Ps or by making the increment larger.

Once a set of WEM-scanned images is made for a range of velocity percentages, a percent velocity can be picked based on the focused amplitude and the geologic consistency of the reflectors. This step requires knowledge of the regional geology. To make it easier to compare images of different velocity percentages, each scan image is redepthed using the reference velocities.

Figure 12a shows the reference velocity model (100% velocity model) that was used for the subsalt WEM scan. Velocities were scaled in the range of 80% to 115% with an increment of 5%, yielding a total of eight WEM volumes. Figure 13 shows three images after redepthing, corresponding to 80%, 100%, and 115% of the reference velocity model. Picking can be done directly on these scanned images or on the scan gathers at each imaging point. The three scan gathers at three imaging points in the lower left side of Figure 12 show that lower velocities generated higher amplitudes. In the lower right side of Figure 12 are three semblancelike pictures (pseudosemblance panels) corresponding to the same imaging points to make picking easier. In addition, updated interval velocities are displayed

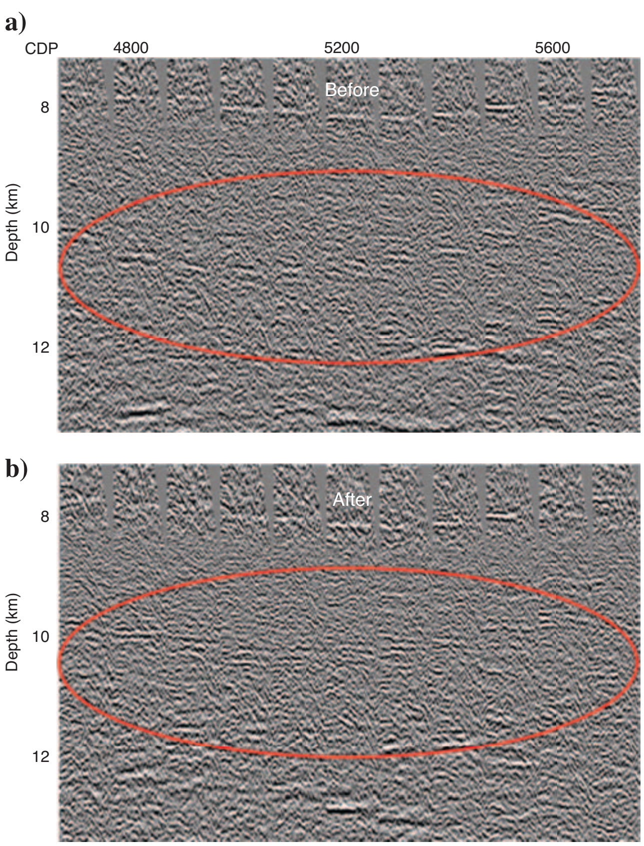

Figure 11. CIP gathers (a) before and (b) after subsalt tomography. In areas of poor S/N, very little improvement is gained by tomography.

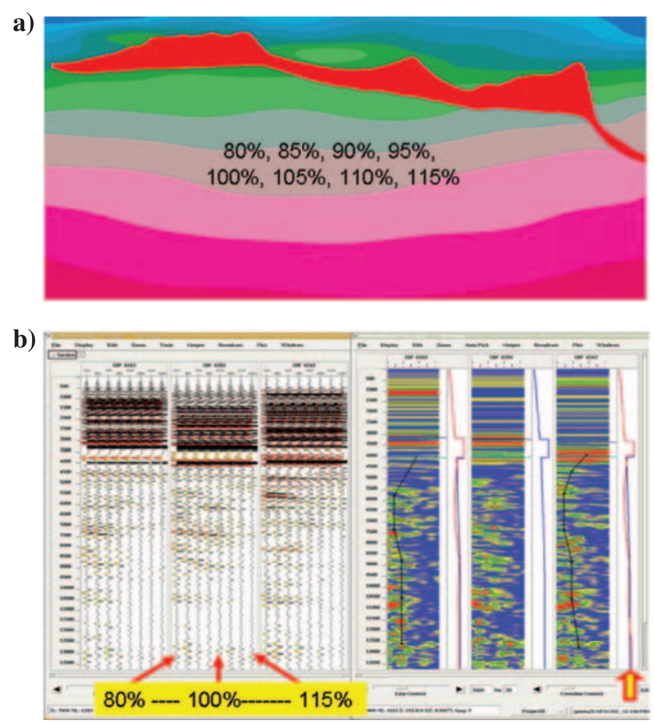

Figure 12. (a) Reference velocity model where velocity below salt is scaled by a percentage from 80% to 115% with a 5% increment; (b) part of the subsalt picking tool which gives real-time feedback for interval velocity update.

instantaneously in comparison with reference velocities to prevent picking an event (such as a residual multiple event) that makes the interval velocity unrealistic. Picking in the scanned images is linked with picking in the scan gathers or pseudosemblance panels to facilitate checking the validity of the picks in terms of interval velocities.

Figure 14 shows the reference velocity model used for the WEM scan and the updated velocity model based on the WEM scan. Velocities just below the left side of the salt body were reduced by about 20% from reference velocities. Velocities below the right side of the salt body were increased somewhat. The faster velocities in this area can be attributed to influence from high-velocity carbonate rocks. Figure 15 shows the PSDM image migrated with the reference model and the image migrated with the updated model. By updating the subsalt velocity model using WEM scan, we enhanced the subsalt image greatly. Not only was continuity of the reflectors improved significantly, but also the dip of the reflectors was lowered, which later was confirmed to be consistent with well data from the area.

Alternative scanning techniques

Although the wave-equation-based subsalt scan technique is effective, the cost of generating multiple volumes of WEM images is still high. To reduce cost, focusing analysis-based DIT scan, an efficient alternative for subsalt scan, was proposed (Wang et al., 2005a; Wang et al., 2006). In DIT scan, we downward continue the wavefield and generate multiple images at each depth by using a nonzero-time (or time-shift) imaging condition (Sava and Fomel, 2006). DIT denotes delayed imaging time or a time shift for imaging.

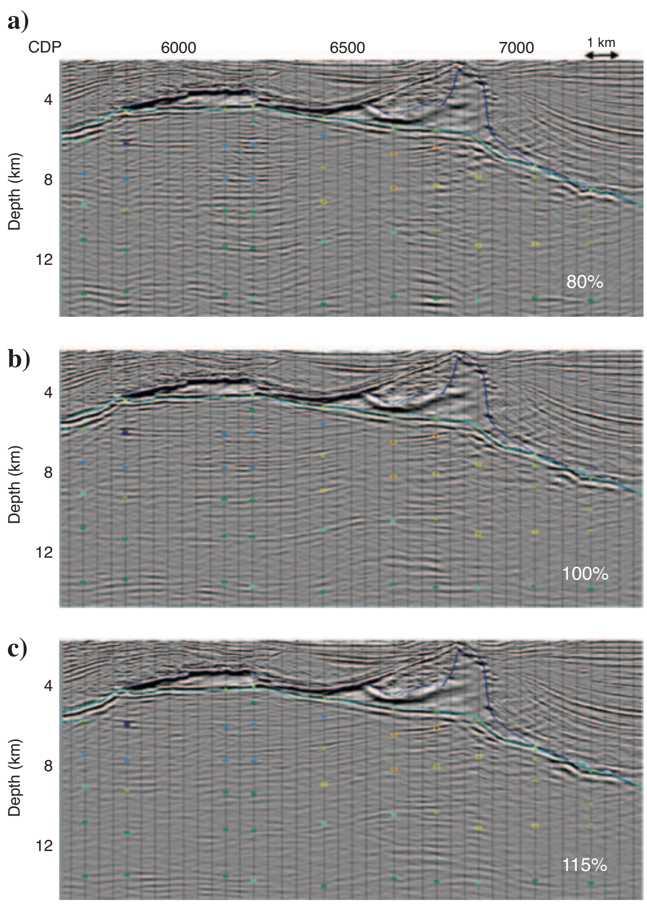

Figure 13. Examples of subsalt WEM scan corresponding to (a) 80%, (b) 100%, and (c) 115% of the reference velocity model in Figure 12a.

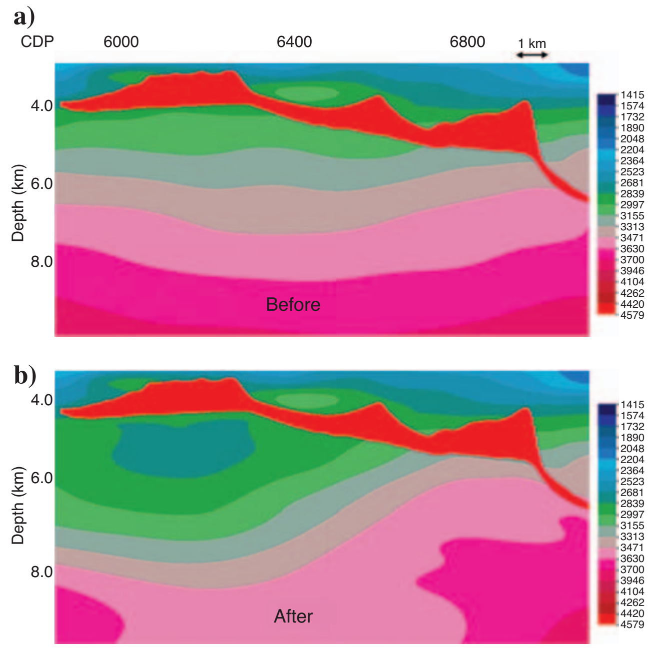

Figure 14. Velocity models (a) before and (b) after subsalt WEM scan. The velocity above the base of salt is the same, but subsalt sediment velocity is quite different.

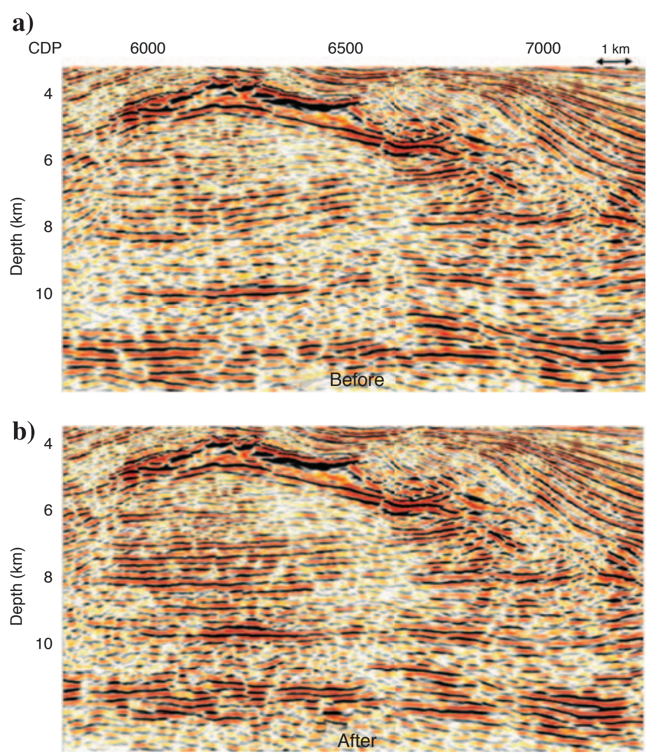

Figure 15. 3D prestack WEM migration images before (a) and (b) after subsalt WEM scan using velocity models in Figure 14. Updated image (b) gives a more geologically reasonable image and matches well-derived dip information more closely.

Because applying a time-shift imaging condition does not add much computation, we can generate very dense DIT scans with slightly more than the cost of running a single prestack WEM. The cost of generating a standard WEM scan is linearly proportional to the number of scans to be generated. In a typical subsalt scan project, we can generate 21 scans using a DIT scan technique at less than half the cost of generating seven to nine WEM scans. Figure 16 shows three images corresponding to DIT equal to -300 ms, 0 ms, and 300 ms, respectively. Migration was carried out with the reference velocity model shown in Figure 12. Note that reflectors below salt were focused better with a 300-ms time shift.

DIT scan gathers can be converted to pseudosemblance panels for picking optimal DIT values that can be used to generate an optimally focused depth image. This procedure is very similar to that with WEM scan gathers. One difference is that we pick a DIT value instead of a velocity percentage. Figure 17 shows a WEM image corresponding to DIT $=$ 0 ms and a composite WEM image using picked DITs from the subsalt DIT scan. Note that subsalt reflectors are more continuous in the composite image. Because it is almost impossible to build a “perfect” velocity model for field data, DIT scan is an excellent tool to improve the final image without adding much computation.

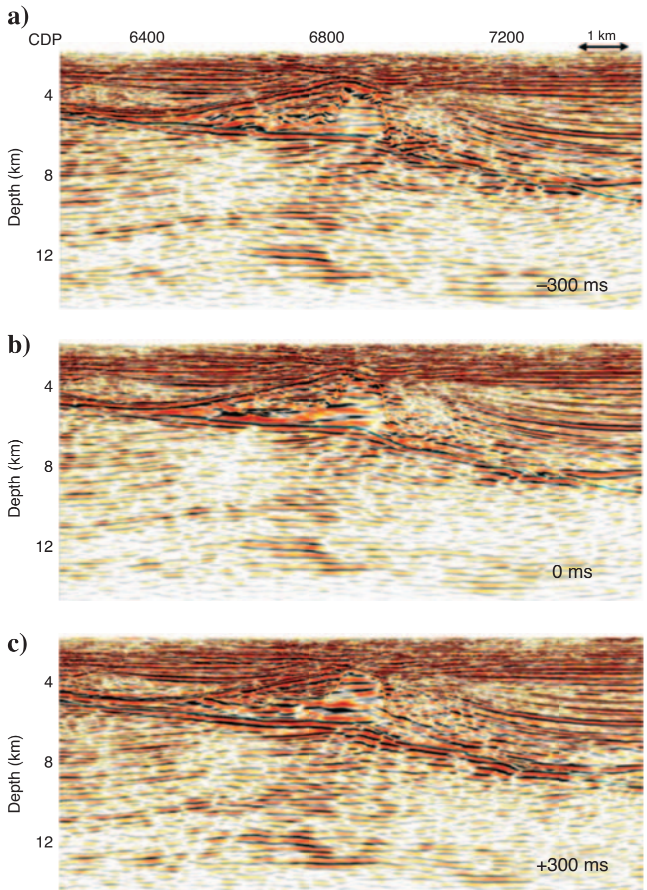

Figure 16. Examples of subsalt DIT scan corresponding to DIT equal to (a) -300 ms, (b) 0 ms, and (c) $+300$ ms, using the reference velocity model.

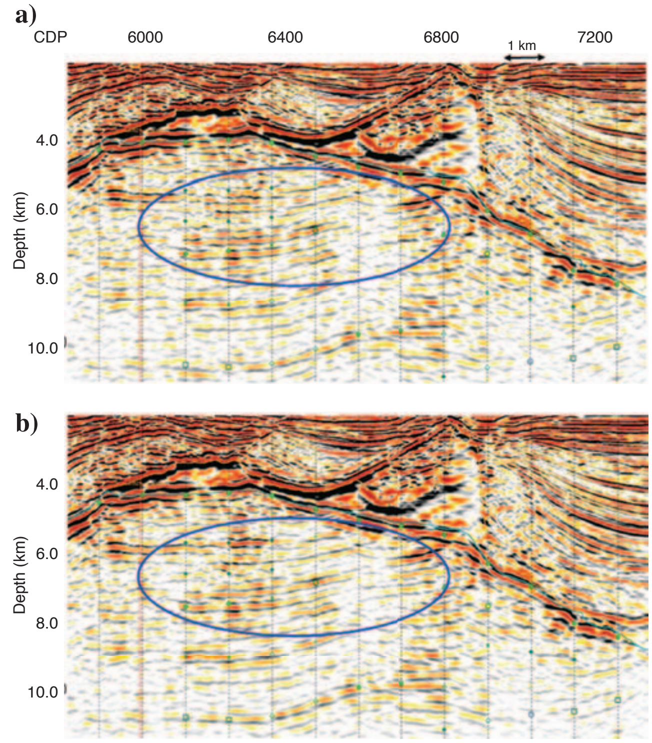

Figure 17. Examples of subsalt wave-equation-based DIT scans. (a) WEM image corresponding to DIT $=$ 0 and (b) composite image using picked DIT on subsalt DIT scans.

CONCLUSION

There are three critical steps in subsalt imaging: estimation of velocities above the salt, definition of salt geometry, and subsalt velocity update. Routinely, velocities above salt are determined by using grid tomography. However, when there is a high-velocity layer, hybrid tomography works better by introducing a layer constraint to tomographic inversion.

Once the velocities above salt are determined accurately, interpreting the top of salt is relatively straightforward. However, interpreting the base of salt is often difficult and tedious because residual multiples obscure the base or it is missing in the image because of lack of illumination. When subsalt reflections are discernible, however, one can combine demigration and fast beam migration to test scenarios for the base of salt and determine the base by using reflector continuity or geologic consistency. In addition, reverse time migration can be used to improve salt boundaries further when there are turning or prism waves from steep or overturned salt flanks (Jones et al., 2007). We illustrated the use of demigration to a subsurface datum, which makes picking of dips much easier for fast beam migration to determine the base of salt. Obtaining a correct salt shape is critical to subsalt velocity update because the techniques for subsalt velocity update can compensate for errors in salt geometry.

To update subsalt velocities, conventional tomography should work well with a slight modification such as freezing velocities above the base of salt or ray tracing performed from the base of salt instead of from the surface. Of course, there should be coherent subsalt reflections and a sufficient range of reflection angles for subsalt tomography. In areas of poor illumination, data-driven tomography sometimes can fall off the trend and create problems converging to the correct velocity model. When subsalt reflections are not defined well or the range of reflection angle is limited, one might have to rely on a brute-force approach based on parameter scan. We illustrated the use of subsalt WEM scan to update subsalt velocities to improve the WEM image and the use of DIT scan to enhance the final image. When scan-based techniques fail to generate useable subsalt images, one might have to consider new data acquisition with wide azimuth to ensure illumination of subsalt targets.

ACKNOWLEDGMENTS

We would like to thank August Lau and Chuan Yin at Apache Corporation for their valuable input for one of our proprietary projects. We thank Zhiming Li, Laurie Geiger, Liz Beal, Steve Hightower, Duryodhan Epili, and Abu Chowdhury for providing their valuable insights and their help in generating some of the figures. Many people made good contributions toward developing some of the tools used to produce some of the data examples. We specifically acknowledge the following contributors: Manhong Guo, Sampath Gajawada, Jean Ji, Weihong Fei, and Jing Xie. We express our sincere appreciation to Bill Harlan, Jennifer Lewis, Fuhao Qin, and anonymous reviewers for excellent suggestions to improve the manuscript. Finally, we thank TGS-NOPEC management for permission to publish this paper.

REFERENCES

Campbell, A. G., E. Evans, D. Judd, I. F. Jones, and S. Elam, 2006, Hybrid girded tomography in the southern North Sea: 75th Annual International Meeting, SEG, Expanded Abstracts, 2538–2541.

Dirks, V., B. Wang, D. Epili, D. Wheaton, P. Guillaume, F. Audebert, and N. Chazalnoel, 2005, Automatic, dense and volumetric picking for high-resolution 3D tomographic model building: 75th Annual International Meeting, SEG, Expanded Abstracts, 2538–2541.

Epili, D., W. Fei, J. Xie, D. Teixeira, and Y. Kim, 2007, Efficient 3D grid tomography using kinematic iterations: 76th Annual International Meeting, SEG, Expanded Abstracts, 3004–3007.

Fei, W., D. Epili, and Y. Kim, 2006, Practical aspects of parsimonious migration for velocity tomography: 76th Annual International Meeting, SEG, Expanded Abstracts, 2465–2468.

Fei, W., and G. McMechan, 2006, 3D common-reflection-point-based seismic migration velocity analysis: Geophysics, **71**, no. 5, S161–S167.

Gao, F., P. Zhang, B. Wang, and V. Dirks, 2006, Fast beam migration — A step toward interactive imaging: 76th Annual International Meeting, SEG, Expanded Abstracts, 2470–2473.

Gray, S., 2005, Gaussian beam migration of common shot records: Geophysics, **70**, no. 4, S71–S77.

Guillaume, P., N. Chazalnoel, A. Talaalout, X. Zhang, D. Epili, and V. Dirks, 2003, 3D finite-offset depth tomography model building: Green Canyon, Gulf of Mexico: 73rd Annual International Meeting, SEG, Expanded Abstracts, 438–441.

Hill, N. R., 1990, Gaussian beam migration: Geophysics, **55**, 1416–1428.

Hua, B. L., and G. A. McMechan, 2001, Parsimonious 2-D poststack Kirchhoff depth migration: Geophysics, **66**, 5, 1497–1503.

———, 2003, Parsimonious 2D prestack Kirchhoff depth migration: Geophysics, **68**, 1043–1051.

Jones, I., M. C. Goodwin, I. D. Berranger, H. Zhou, and P. A. Farmer, 2007, Application of anisotropic 3D reverse time migration to complex North Sea imaging: 77th Annual International Meeting, SEG, Expanded Abstracts, 2140–2143.

Kim, Y., C. M. Samuelsen, and T. A. Hauge, 1996, Efficient velocity model building for prestack depth migration: The Leading Edge, **15**, 751–753.

Liu, J., F. Gao, P. Zhang, and V. Dirks, 3D beam based prestack redatuming for efficient subsalt velocity analysis: 77th Annual International Meeting, SEG, Expanded Abstracts, 2802–2805.

Lu, R., M. Willis, X. Campman, and J. Ajo-Franklin, 2007, Redatumming through a salt canopy — Another salt flank imaging strategy: 77th Annual International Meeting, SEG, Expanded Abstracts, 3054–3057.

Mosher, C., E. Keskula, J. Malloy, R. Keys, H. Zhang, and S. Jin, 2007, Iterative imaging for subsalt interpretation and model building: The Leading Edge, **26**, 1424–1428.

Reasnor, M. D., 2007, Salt interpretation practices for depth imaging in the Gulf of Mexico: The Leading Edge, **26**, 1438–1441.

Sava, P., and S. Fomel, 2006, Time-shift imaging condition in seismic migration: Geophysics, **71**, no. 6, S209–S217.

Sayers, C., and D. Herron, 2007, Introduction to this special section: Subsalt exploration: The Leading Edge, **26**, 1404–1405.

Schuster, J., and M. Zhou, 2006, A theoretical overview of model-based and correlation-based redatuming methods: Geophysics, **71**, no. 4, SI103–SI110.

Singer, P., 2005, Subsalt imaging: Is the salt winning? Presented at the 2005 SEG/EAGE Summer Workshop.

Stork, C., 1992, Reflection tomography in the postmigrated domain: Geophysics, **57**, 680–692.

Sun, Y. H., F. H. Qin, S. Checkles, and J. P. Leveille, 2000, 3-D prestack Kirchhoff beam migration for depth imaging: Geophysics, **65**, 1592–1603.

Sun, H., and J. Schuster, 2003, 2D wavepath migration: Geophysics, **66**, 1528–1537.

Wang, B., F. Audebert, D. Wheaton, and V. Dirks, 2006a, Subsalt velocity analysis by combining wave equation based redatuming and Kirchhoff based migration velocity analysis: 76th Annual International Meeting, SEG, Expanded Abstracts, 2440–2444.

Wang, B., V. Dirks, P. Guillaume, F. Audebert, and D. Epili, 2006b, A 3D subsalt tomography based on wave-equation migration-perturbation scans: Geophysics, **71**, no. 2, E1–E6.

Wang, B., V. Dirks, P. Guillaume, F. Audebert, A. Hou, and D. Epili, 2004, 3D sub-salt tomography based on wave equation migration perturbation scans: 74th Annual International Meeting, SEG, Expanded Abstracts, 2375–2378.

Wang, B., and K. Pann, 1996, Kirchhoff migration of seismic data compressed by matching pursuit decomposition: 66th Annual International Meeting, SEG, Expanded Abstracts, 1642–1645.

Wang, B., K. Pann, and R. A. Meek, 1995, Macro velocity model estimation through model-based globally-optimized residual-curvature analysis: 65th Annual International Meeting, SEG, Expanded Abstracts, 1084–1087.

Wang, B., F. Qin, F. Audebert, and V. Dirks, 2005a, A fast and low cost alternative to subsalt wave equation migration perturbation scans: 75th Annual International Meeting, SEG, Expanded Abstracts, 2257–2260.

Wang, B., F. Qin, V. Dirks, P. Guillaume, F. Audebert, and D. Epili, 2005b, 3D grid tomography based on focusing analysis: 67th Conference and Exhibition, EAGE, Extended Abstracts.

———, 2005c, 3D finite angle tomography based on focusing analysis: 75th Annual International Meeting, SEG, Extended Abstracts, 2546–2549.

Wang, B., D. Wheaton, F. Audebert, and V. Dirks, 2006, Separation of focusing and positioning effects using wave equation based focusing analysis and post-stack modeling: 76th Annual International Meeting, SEG, Expanded Abstracts, 2646–2649.

Zhou, H., J. Guo, and J. Young, 2001, An alternative residual-curvature velocity updating method for prestack depth migration: 71st Annual International Meeting, SEG, Expanded Abstracts, doi:10.1190/1.1816776.